Acta Mech 226, 1621–1640 (2015)
DOI 10.1007/s00707-014-1273-3

A. Ortiz-Bernardin · D. Sfyris

A finite element formulation for stressed bodies with continuous distribution of edge dislocations

Received: 13 June 2013 / Revised: 16 June 2014 / Published online: 26 November 2014

Abstract On using Noll's theory of materially uniform but inhomogeneous bodies, a nonlinear finite element method for treating a body with a continuous distribution of edge dislocations is presented. To this end, we use the multiplicative decomposition of the deformation gradient, which is herein referred to as the $\mathbf{F}^*$ decomposition. The nonlinear finite element method is devised starting from a hyperelastic-like strain energy as a function of $\mathbf{F}^*$. By making a specific assumption for the uniform reference, we model a bar with a continuous distribution of edge dislocations parallel to the plane that defines a cross section of the bar and with the Burgers vector along the axial direction of the bar. This body is subjected to pure tension along its axial direction, and we examine how the presence of the defects affects the elastic solution. The numerical results are juxtaposed with the analogous ones that are obtained from the corresponding elastic material. It appears that the field of the defects affects the nonlinearity in the stress–strain response in the sense that stresses grow "faster" pointwise in the dislocated body. Thus, if a definite yield limit exists, it is approached faster by the dislocated model at hand due to the presence of defects in the as-received body. We also focus our attention in the case of only one dislocation and conclude that near the core region our model predicts finite stresses. Finally, a close loop consisting of a screw and an edge segment is treated within this theory. As expected, it appears that near the loop stresses are concentrated. Our framework is valid for a body with a frozen distribution of dislocations, namely the defects exist, but are not allowed to move. So, essentially, it models an elastic body with internal stresses resulting from dislocations. Thus, our approach is assumed to be one step before the initiation of plasticity, and we are interested in how the field of the inhomogeneity that arises from a fixed distribution of defects affects the elastic solution. This is the first attempt to apply the multiplicative decomposition to problems with dislocations in the literature, thereby highlighting that Noll's abstract approach can be put into the perspective of standard engineering computations.

1 Introduction

The theory of materially uniform but inhomogeneous bodies has been presented by Noll [36] in a seminal paper and expanded by Wang [50]. A recent monograph by Epstein and Elzanowski [18] (see [17]) describes in a thorough and apt way this theory while giving various extensions and applications. The theory of materially uniform but inhomogeneous bodies attempts to describe a body with a continuous distribution of dislocations.

This theory has attracted some attention in the dislocations literature among years. Bertram [7] presented the theoretical guidelines for building up a continuum plasticity framework starting from the notion of material

A. Ortiz-Bernardin
Department of Mechanical Engineering, University of Chile, Beauchef 850, Santiago 8370448, Chile

D. Sfyris (✉)
Foundation for Research and Technology, Institute of Chemical Engineering Sciences, Patras 26504, Greece
E-mail: dsfyris@iceht.forth.gr
Tel.: +30 2610 961 259

isomorphism. He also extended this framework to the case when thermal effects are taken into account [8,9]. The works of Svendsen [48,49] are along the same direction. Among other things, anisotropy effects are discussed as well as how hardening can be incorporated into the theory. The role of plastic dissipation, material symmetry and Illyshin postulate has been tackled by Gupta et al. [25,26] with a view toward the evolution of dislocations in the body. The important paper of Epstein and Maugin [21] highlights the role played by Eshelby's stress tensor. A framework for the geometrical structure of anelasticity has been given by the same authors [22]. The constitutive character of plastic deformation has been the topic in the work of Cleja-Tigoiu and Soos [12].

The geometrical literature related to this theory is vast. It starts with the seminal works of Kondo [28], Bilby et al. [10] and Kröner [30] in the mid of the previous century. In the recent literature, Epstein and coworkers extended the theory of inhomogeneities to bodies with microstructure [16] as well as to Cosserat materials [19,20]. Based on a variational framework, Le and Stumpf [31,33] gave a new set of field equations for the case where the field of the defects varies with time, thereby producing plasticity. The determination of the intermediate configuration when the elastic strain and the dislocation density are given has been also treated by Le and Stumpf [32]. The approach of Steinmann [47] exploits the role of the kinematical necessary dislocations in the positiveness of the plastic dissipation.

In the very recent literature, the work of Yavari and Goriely [53] uses the theory of Cartan's moving frames for constructing the intermediate configuration in dislocation theories. Also, the calculation of the field of the internal stresses is one of the topics in Yavari and Goriely [53]. Our approach based on Noll's theory can be seen in Sfyris et al. [46] and Sfyris [41–45].

On the other hand, one may propose a continuum theory of dislocations where the starting point is the dislocations field and not the plastic deformation. In a series of papers, Acharya and coworkers proposed a framework for giving a plasticity theory starting from the notion of dislocation. After giving a complete system of equations for the fully dynamical problem [1–3], they solve numerically many interesting cases in the linear regime [39,40]. An approach for linking the continuum plasticity framework with the theory of dislocations is also given by averaging the equations of dislocations mechanics, and relation is made with the basic ingredients of continuum plasticity [4,5]. Earlier approaches that employ an evolution equation for the dislocation density may be found in the works of Kosevich [29], Kröner [30], Mura [35] and Willis [51].

Within the linear continuum theory of dislocations, the finite element method, as well as an atomistic modeling, has been used in the works of Dluzewski et al. [13–15]. The finite element method using enrichment functions to model the dislocation as a line or surface of discontinuity is tackled in the works of Gracie et al. [23,24] and Belytschko and Gracie [6]. Also, it is worth mentioning the work of Y. Basar [52] in multilayer analysis as well as the work of Palmov [37] in viscoplasticity at large deformations.

The present paper is concerned with a nonlinear finite element analysis of a bar that is subjected to uniaxial tension and that contains a continuous distribution of edge dislocations. Such dislocations are modeled using Noll's theory of materially uniform but inhomogeneous bodies [36]. The field of the inhomogeneity is given a specific form that pertains to a continuous distribution of edge dislocations [46]. We assume that the defects are not allowed to move with respect to the material; therefore, plasticity is not produced. Essentially, the effective uncoupling [12] of the elastic and the plastic deformation, inherent in the multiplicative decomposition, enables to vary the elastic field without altering the field of the defects. The continuously dislocated body is subjected to a tensional loading, and we examine the role played by the field of the defects in the elastic solution in the geometrically and materially nonlinear regime.

We formulate a nonlinear finite element method to tackle this problem. To this end, we use the multiplicative decomposition of the deformation gradient, which is herein referred to as the $\mathbf{F}^*$ decomposition. In this approach, a hyperelastic-like strain energy is written in terms of $\mathbf{F}^*$ and used to develop the weak and linearized weak forms. As a result, a standard hyperelastic code can be used with few changes to model dislocations under Noll's framework with our method. The outcome is juxtaposed with the corresponding purely elastic problem. The corresponding elastic material is defined in Sfyris [43]. The energy of such a material equals the energy of the dislocated material when the defects are absent, namely when the material uniformity is set equal to the unit tensor. The solution of the elastic problem is compared with that of the corresponding dislocated problem. This way, we highlight the role played by a fixed distribution of inhomogeneities (that arises from dislocations) in the elastic solution of a bar under uniaxial tension.

On using the $\mathbf{F}^*$ decomposition finite element method, we find that due to the presence of defects the nonlinearity in the stress–strain response is altered in the sense that for the dislocated model stresses grow faster with strains. Thus, if a definite yield limit for the material exists, this is approached faster by the dislocated body. Of course, due to the inhomogeneity, the analysis is pointwise, so there are other points (and regions) where the "velocity" of the nonlinearity is affected less. This change signifies the localization of the

deformation that occurs as an outcome of the defects' presence—there are zones where the dislocated bar arrives to the yield limit, while other regions remain at the elastic regime when a homogeneous yield criterion is used.

From the numerical point of view, the field of defects is introduced by specifying the inhomogeneity (which is treated as a given data) at every Gauss point of the finite element mesh. Thus, the boundary conditions are not altered by the presence of the defects, to wit, the elastic and the dislocated problem are having the same boundary conditions. Of course, the boundary nodes of the dislocated body are affected more from the loading than their elastic counterparts are.

Attention is then focused to modeling of only one dislocation threading the bar in the prism of Noll's framework. The similar case of a single screw dislocation has been treated in the work of Rosakis and Rosakis [38] with the fundamental difference that these authors model the defect as a line of singularity in the elastic field. We emphasize that in our approach the elastic field remains smooth (i.e., it suffers no jumps), whereas all the "bad properties" (Curl not free) that model the dislocation line are carried by the uniform reference.

Also in the literature of single screw dislocations, Acharya [1], using notions from exterior calculus, evaluates the internal stress field when a neo-Hookean material is considered. After constructing the relaxed manifold based on Cartan's frames, Yavari and Goriely [53] calculate the field of internal stresses for a single screw dislocation. The basic difference between these approaches and our approach relies in that in our method the external loading is taken into account in addition to the internal field of stresses. Thus, not only the dislocations exist, but also the body is loaded. The solution is then compared with the purely elastic one, namely as if the defects were not present. Finally, we remark that in our method the dislocations are not modeled using distributions, but rather Gauss points that discretely constitute a line are selected in the medium, and the value of the uniform reference is specified at these points.

Along the same lines, a closed loop is also treated. The loop consists of an edge and a screw segment. The edge segment corresponds to a dislocation line parallel to the plane that defines a cross section of the bar and with the Burgers vector along the axial direction of the bar. The screw segment is described by a different map of the inhomogeneity [46] and corresponds to a screw dislocation with both the Burgers vector and the dislocation line along the axial direction of the bar. The screw part is needed in order for the loop to be closed.

The paper is structured as follows. Section 2 starts by defining a materially uniform but inhomogeneous body following the ideas of Noll and continues by giving the weak formulation for the problem at hand. Section 3 is devoted to the linearization of the weak form, whereas in Sect. 4, the corresponding discretized equations are presented. Section 5 provides numerical examples using our method; Sect. 5.1 treats the continuous distribution of dislocations; Sect. 5.2 tackles the problem of only one edge dislocation threading the bar; and Sect. 5.3 treats the closed loop. The article ends in Sect. 6 with some concluding remarks.

2 Weak form

Let $\mathcal{B}_R$ be the reference configuration of a body, whereas the current configuration is denoted by $\mathcal{B}_C$. The usual space of admissible deformations is considered:

$$\mathscr{D} = \{\chi : \Omega \to \mathbb{R}^3 \mid \det \mathbf{F} > 0,\ \chi = \bar{\chi} \ \text{ on } \Gamma_\chi\}, \tag{1}$$

where $\Omega \subseteq \mathcal{B}_R \in \mathbb{R}^3$ is an open-bounded domain on the initial (reference) configuration with boundary Γ, and χ is the mapping that defines the displacement of a particle from its initial position $\mathbf{X}$ in $\mathcal{B}_R$ to its current position $\mathbf{x}$ in $\mathcal{B}_C$, i.e., $\mathbf{u} = \chi(\mathbf{X}) - \mathbf{X} = \mathbf{x} - \mathbf{X}$. On the other hand, Γ_χ is the portion of the boundary where the deformation $\bar{\chi}$ is prescribed. The vectors of external body forces $\mathbf{f}_0$ and external surface forces $\mathbf{t}_0$ are assumed to be independent of the motion. As usual, the gradient of the mapping χ, denoted by $\mathbf{F}$, is the deformation gradient tensor given by

$$\mathbf{F} = \frac{\partial \chi}{\partial \mathbf{X}}. \tag{2}$$

For an inhomogeneous body, the elastic energy is a function of $\mathbf{F}$ and $\mathbf{X}$, namely $\bar{W}$. According to Noll [36], if there exists a function $\bar{W}_U$ such that the elastic energy can be written as

$$\bar{W}(\mathbf{F}, \mathbf{X}) = \bar{W}_U(\mathbf{FK}), \tag{3}$$

then the material is called materially uniform. In this paper, the argument of $\bar{W}_U$ in the right-hand side of Eq. (3) is referred to as the $\mathbf{F}^*$ (multiplicative) decomposition[1], to wit,

$$\mathbf{F}^* = \mathbf{F}\mathbf{K}, \tag{4}$$

where $\mathbf{K}$ describes inhomogeneities that arise due to a fixed distribution of dislocations [46]. Thus, $\mathbf{F}^*$ can be thought as a modified deformation gradient tensor. Due to its modified character, the energy and quantities such as stresses and strains adopt a modified character as well. The finite element derivations need to be elaborated in a manner that is consistent with these modifications.

Using standard invariance arguments, the energy can be expressed as [34]

$$W(\mathbf{C}, \mathbf{X}) = W_U((\mathbf{F}^*)^{\mathrm{T}}\mathbf{F}^*) = W_U(\mathbf{C}^*) \equiv W_U^* \tag{5}$$

where $\mathbf{C} = \mathbf{F}^T\mathbf{F}$ is the right Cauchy–Green deformation tensor and $\mathbf{C}^* = \mathbf{F}^{*T}\mathbf{F}^*$ is the modified right Cauchy–Green deformation tensor. Accordingly, the modified second Piola–Kirchhoff stress tensor takes the form

$$\mathbf{S}(\mathbf{C}^*) = 2\frac{\partial W_U(\mathbf{C}^*)}{\partial \mathbf{C}^*} = \frac{\partial \tilde{W}_U(\mathbf{E}^*)}{\partial \mathbf{E}^*} \equiv \mathbf{S}^* \tag{6}$$

where $\mathbf{E}^*$ is the modified strain tensor produced by $\mathbf{F}^*$, namely

$$\mathbf{E}^* = \frac{1}{2}\left[(\mathbf{F}^*)^{\mathrm{T}}\mathbf{F}^* - \mathbf{I}\right]. \tag{7}$$

The decisive answer to the existence or not of the dislocations is given by the field $\mathbf{K}$. When $\mathbf{K}$ can be written globally as a gradient, then dislocations are absent, and the material is purely elastic [36,50]. In the opposite case, where $\mathbf{K}$ cannot be written globally as the gradient of some point mapping, then dislocations exist in the body and the material is called inhomogeneous. From the physical point of view, Eq. (3) reveals that the inhomogeneity of the body is only through $\mathbf{K}$, which describes the relaxation procedure from the internal stresses due to the presence of dislocations [21]. The outcome of this relaxation procedure is a collection of small relaxed pieces, denoted by $\mathcal{B}_U$.

The source of the dislocation density is the deviation of $\mathbf{K}$ from being Curl-free. The dislocation density tensor is a measure of this deviation and is defined as [29,30]

$$\hat{\alpha}_{C\alpha} = \epsilon_{ABC} K^{-1}_{\alpha A,B} \tag{8}$$

for its two point expression, whereas for the fully material expression we have [29,30]

$$\alpha_{DC} = \hat{\alpha}_{D\alpha} K^T_{\alpha C}. \tag{9}$$

So, the field $\mathbf{F}$ describes the elastic part of the theory, whereas $\mathbf{K}$ describes the part related with the defects. These quantities are assumed to be independent with respect to each other. The dependent variable is $\mathbf{F}^*$, which maps $\mathcal{B}_U$ to $\mathcal{B}_C$ (see Fig. 1). In our derivations, indicial capital Latin notation stands for quantities in $\mathcal{B}_R$, whereas small-case Latin indices are used for quantities in $\mathcal{B}_C$, and small-case Greek indices are used for quantities in $\mathcal{B}_U$. So, with respect to indices, we have $F^*_{i\alpha} = F_{iA}K_{A\alpha}$.

In the material (reference) configuration, the following modified potential energy functional arises:

$$\Pi^*(\chi) = \int_\Omega \tilde{W}_U(\mathbf{E}^*(\chi))\,\mathrm{d}\Omega - \int_\Omega \mathbf{f}_0 \cdot \chi\,\mathrm{d}\Omega - \int_{\Gamma_t} \mathbf{t}_0 \cdot \chi\,\mathrm{d}\Gamma \tag{10}$$

where $\tilde{W}_U(\mathbf{E}^*(\chi))$ is the modified strain energy function.

The virtual variation of Eq. (10) in the arbitrary direction $\mathbf{v} \in \mathscr{V} = \{\mathbf{v}{:}\Omega \to \mathbb{R}^3 \mid \mathbf{v} = \mathbf{0} \text{ on } \Gamma_\chi\}$ yields

$$\begin{aligned}\delta\Pi^* = D\Pi^*[\mathbf{v}] &= \int_\Omega \frac{\partial \tilde{W}_U(\mathbf{E}^*)}{\partial \mathbf{E}^*}{:}\delta\mathbf{E}^*\,\mathrm{d}\Omega - \int_\Omega \mathbf{f}_0 \cdot \mathbf{v}\,\mathrm{d}\Omega - \int_{\Gamma_t} \mathbf{t}_0 \cdot \mathbf{v}\,\mathrm{d}\Gamma \\ &= \int_\Omega \mathbf{S}^*{:}\delta\mathbf{E}^*\,\mathrm{d}\Omega - \int_\Omega \mathbf{f}_0 \cdot \mathbf{v}\,d\Omega - \int_{\Gamma_t} \mathbf{t}_0 \cdot \mathbf{v}\,\mathrm{d}\Gamma.\end{aligned} \tag{11}$$

[1] The $\mathbf{F}^*$ deformation gradient tensor is decomposed into two parts, an elastic one and a dislocated one.

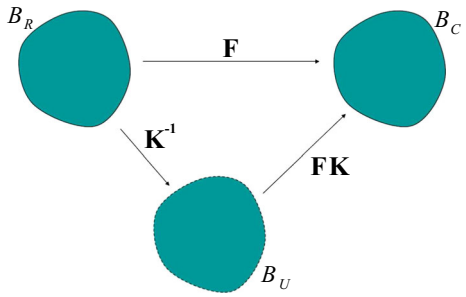

Fig. 1 Configurations that are used in the theory of materially uniform but inhomogeneous bodies

In Eq. (11), the tensor $\mathbf{E}^*$ written with respect to indices has the form

$$E^*_{\beta\alpha} = \frac{1}{2}\left[K^{\mathrm{T}}_{\beta A} F^{\mathrm{T}}_{Aj} F_{jB} K_{B\alpha} - \delta_{\beta\alpha}\right]. \tag{12}$$

Taking the variation in Eq. (12) leads to

$$\delta E^*_{\beta\alpha} = DE^*_{\beta\alpha}[\mathbf{v}] = \frac{1}{2}\left[K^{\mathrm{T}}_{\beta A} DF^{\mathrm{T}}_{Aj}[\mathbf{v}] F_{jB} K_{B\alpha} + K^{\mathrm{T}}_{\beta A} F^{\mathrm{T}}_{Aj} DF_{jB}[\mathbf{v}] K_{B\alpha}\right], \tag{13}$$

since the field of the defects does not alter, namely $D\mathbf{K}[\mathbf{v}] = 0$. This assumption is crucial and rests on the effective uncoupling of the elastic and the plastic parts [12]. It signifies that dislocations are fixed within the material; thus, no further plasticity is produced. For the variation of the elastic field (see, for instance, Bonet and Wood [11]), we have

$$DF_{iA}[\mathbf{v}] = \nabla_A v_i. \tag{14}$$

So, collectively the variation of the strain renders

$$\begin{aligned}\delta E^*_{\beta\alpha} = DE^*_{\beta\alpha}[\mathbf{v}] &= \frac{1}{2}\left[K^{\mathrm{T}}_{\beta A}(\nabla_A v_j)^{\mathrm{T}} F_{jB} K_{B\alpha} + K^{\mathrm{T}}_{\beta A} F^{\mathrm{T}}_{Aj} \nabla_B v_j K_{B\alpha}\right] \\ &= \frac{1}{2}\left[K^{\mathrm{T}}_{\beta A}\left\{(\nabla_A v_j)^{\mathrm{T}} F_{jB} + F^{\mathrm{T}}_{Aj}\nabla_B v_j\right\} K_{B\alpha}\right] \\ &= K^{\mathrm{T}}_{\beta A}\left\{F^{\mathrm{T}}_{Aj}\nabla_B v_j\right\}_{\mathrm{sym}} K_{B\alpha}\end{aligned} \tag{15}$$

where the tensor within curly brackets in the last equality is symmetric with respect to the indices A and B and corresponds to the variation of the strain used in pure elasticity problems.

With the help of Eq. (15), the first integrand of the variation in Eq. (11) takes the form

$$\begin{aligned}S^*_{\alpha\beta}{:}\delta E^*_{\beta\alpha} &= S^*_{\alpha\beta}{:}\left[K^{\mathrm{T}}_{\beta A}\left\{F^{\mathrm{T}}_{Aj}\nabla_B v_j\right\}_{\mathrm{sym}} K_{B\alpha}\right] \\ &= \left[K_{A\beta} S^*_{\alpha\beta} K^{\mathrm{T}}_{\alpha B}\right]{:}\left\{F^{\mathrm{T}}_{Aj}\nabla_B v_j\right\}_{\mathrm{sym}}.\end{aligned} \tag{16}$$

In the last equality, the following operation between tensors of second order has been used twice [27]:

$$\mathbf{R}{:}(\mathbf{ST}) = (\mathbf{S}^{\mathbf{T}}\mathbf{R}){:}\mathbf{T} = (\mathbf{RT}^{\mathbf{T}}){:}\mathbf{S}. \tag{17}$$

A careful look at Eq. (16) reveals that the production of virtual power is done by the second Piola–Kirchhoff stress tensor, which is computed as follows:

$$\mathbf{S} = \mathbf{K}\mathbf{S}^*\mathbf{K}^{\mathrm{T}}. \tag{18}$$

This is reasonable since the dislocations are not allowed to move, so there are only elastic variations. Thus, on collecting terms, the virtual variation becomes

$$\delta\Pi^* = \int_\Omega \mathbf{S}{:}\left\{\mathbf{F}^T\nabla\mathbf{v}\right\}_{\mathrm{sym}}\mathrm{d}\Omega - \int_\Omega \mathbf{f}_0\cdot\mathbf{v}\,\mathrm{d}\Omega - \int_{\Gamma_t}\mathbf{t}_0\cdot\mathbf{v}\,\mathrm{d}\Gamma. \tag{19}$$

The last equation reveals the simplicity of the method: The standard virtual work is obtained, and the only change that needs to be taken into account for the finite element implementation is the operation given in Eq. (18). This operation also affects the linearization of the weak form. This is dealt with in the next section.

3 Linearized weak form

The linearized weak form in the direction of the displacement increment $\Delta\mathbf{u}$ is given by

$$D\Pi^*[\mathbf{v}] + D^2\Pi^*[\mathbf{v}, \Delta\mathbf{u}] = 0. \tag{20}$$

The directional derivative in the direction $\Delta\mathbf{u}$ (namely the second variation of Π^*) renders after some calculations

$$D^2\Pi^*[\mathbf{v}, \Delta\mathbf{u}] = \int_\Omega \delta\mathbf{E}{:}\mathcal{C}{:}D\mathbf{E}[\Delta\mathbf{u}]\,\mathrm{d}\Omega + \int_\Omega \mathbf{S}{:}D\delta\mathbf{E}[\Delta\mathbf{u}]\,\mathrm{d}\Omega \tag{21}$$

where the fourth-order tensor $\mathcal{C}$ denotes the elasticity of the dislocated material defined as (Sfyris [41,43])

$$\begin{aligned}\mathcal{C} &= (\mathbf{K}\otimes\mathbf{K}) : \frac{\partial^2 \tilde{W}_U(\mathbf{E}^*)}{\partial\mathbf{E}^*\partial\mathbf{E}^*} : (\mathbf{K}^{\mathrm{T}}\otimes\mathbf{K}^{\mathrm{T}}) = (\mathbf{K}\otimes\mathbf{K}) : \mathcal{C}(\mathbf{E}^*) : (\mathbf{K}^{\mathrm{T}}\otimes\mathbf{K}^{\mathrm{T}}) \\ &= (\mathbf{K}\otimes\mathbf{K}) : \mathcal{C}^* : (\mathbf{K}^{\mathrm{T}}\otimes\mathbf{K}^{\mathrm{T}}).\end{aligned} \tag{22}$$

The last equation in indicial notation reads:

$$\mathcal{C}_{ABCD} = K_{\alpha A}K_{\beta B}\left(\frac{\partial^2 \tilde{W}_U(\mathbf{E}^*)}{\partial\mathbf{E}^*\partial\mathbf{E}^*}\right)_{\alpha\beta\gamma\delta} K^T_{\gamma C}K^T_{\delta D}. \tag{23}$$

The above developments reveal that the finite element implementation is straightforward. In fact, a standard hyperelastic code can be used with few changes, namely the second Piola–Kirchhoff stress is replaced with the one given in Eq. (18), and the material elasticity tensor is replaced with the one given in Eq. (22).

4 Discrete linearized weak form

The discretization of the linearized weak form Eq. (20) leads to the following Newton–Raphson scheme:

$${}^{t+\Delta t}\left(\mathsf{K}_{\mathrm{mat}} + \mathsf{K}_{\mathrm{geo}}\right)^{(i-1)}\,\Delta\mathsf{u}^{(i)} = {}^{t+\Delta t}\mathsf{F} - {}^{t+\Delta t}\mathsf{T}^{(i-1)} = {}^{t+\Delta t}\mathsf{R}^{(i-1)} \tag{24}$$

where $\mathsf{K}_{\mathrm{mat}}$ and $\mathsf{K}_{\mathrm{geo}}$ are the material and geometric global tangent stiffness matrices, respectively; F and T are the external and internal global nodal force column vectors, respectively; R is the residual global nodal force column vector; and $\Delta\mathsf{u}$ is the column vector that contains all the displacement degrees of freedom of the finite element mesh. On the other hand, $t + \Delta t$ denotes the incremental approach, where a solution is known at discrete time t and the solution at discrete time $t + \Delta t$ is sought; the increment Δt corresponds to the load step or load increment. Finally, i stands for the equilibrium iterations within an increment.

The global tangent stiffness matrices as well as the global nodal force column vectors are obtained by assembly of nodal contributions of the finite elements. The following finite element interpolations in the material (reference) configuration of a 8-node hexahedron are considered:

$$\Delta\mathbf{u}_h(\mathbf{X}) = \sum_{a=1}^{8} N_a(\mathbf{X})\Delta\mathbf{u}_a, \tag{25.1}$$

for the trial function, and

$$\mathbf{v}_h(\mathbf{X}) = \sum_{a=1}^{8} N_a(\mathbf{X})\mathbf{v}_a, \tag{25.2}$$

for the test function. In Eq. (25), N_a is the finite element shape function. Thus, after invoking the arbitrariness of nodal variations, the discretization using Eq. (25) yields

$$(\mathsf{R})_a = \int_\Omega N_a\mathbf{f}_0\,\mathrm{d}\Omega + \int_\Gamma N_a\mathbf{t}_0\,\mathrm{d}\Gamma - \int_\Omega \left(\mathsf{B}^0_a\right)^{\mathrm{T}}\mathsf{S}\,\mathrm{d}\Omega \tag{26}$$

for the nodal contribution of the residual nodal force vector,

$$(\mathsf{K}_{\text{mat}})_{ab} = \int_{\Omega} \left(\mathsf{B}_a^0\right)^{\mathrm{T}} \mathsf{C}\mathsf{B}_b^0 \, \mathrm{d}\Omega \tag{27}$$

for the nodal contribution of the material tangent stiffness matrix, and

$$\left(\mathsf{K}_{\text{geo}}\right)_{ab} = \mathbf{I} \int_{\Omega} (\boldsymbol{\nabla}^0 N_a)^{\mathrm{T}} \mathbf{S} (\boldsymbol{\nabla}^0 N_b) \, \mathrm{d}\Omega \tag{28}$$

for the nodal contribution of the geometric tangent stiffness matrix. In the preceding equations,

$$\mathsf{C} = \begin{pmatrix} \mathcal{C}_{1111} & \mathcal{C}_{1122} & \mathcal{C}_{1133} & \mathcal{C}_{1112} & \mathcal{C}_{1113} & \mathcal{C}_{1123} \\ \mathcal{C}_{1122} & \mathcal{C}_{2222} & \mathcal{C}_{2233} & \mathcal{C}_{2212} & \mathcal{C}_{2213} & \mathcal{C}_{2223} \\ \mathcal{C}_{1133} & \mathcal{C}_{2233} & \mathcal{C}_{3333} & \mathcal{C}_{3312} & \mathcal{C}_{3313} & \mathcal{C}_{3323} \\ \mathcal{C}_{1112} & \mathcal{C}_{2212} & \mathcal{C}_{3312} & \mathcal{C}_{1212} & \mathcal{C}_{1213} & \mathcal{C}_{1223} \\ \mathcal{C}_{1113} & \mathcal{C}_{2213} & \mathcal{C}_{3313} & \mathcal{C}_{1213} & \mathcal{C}_{1313} & \mathcal{C}_{1323} \\ \mathcal{C}_{1123} & \mathcal{C}_{2223} & \mathcal{C}_{3323} & \mathcal{C}_{1223} & \mathcal{C}_{1323} & \mathcal{C}_{2323} \end{pmatrix} \tag{29}$$

is the symmetric form of $\mathcal{C}$ using Voigt notation,

$$\mathsf{S} = \begin{pmatrix} S_{11} & S_{22} & S_{33} & S_{12} & S_{13} & S_{23} \end{pmatrix}^{\mathrm{T}} \tag{30}$$

is the symmetric form of $\mathbf{S}$ using Voigt notation, whereas $\mathbf{I}$ is the identity tensor. Finally,

$$\mathbf{B}_a^0 = \begin{bmatrix} F_{11}N_{a,X} & F_{21}N_{a,X} & F_{31}N_{a,X} \\ F_{12}N_{a,Y} & F_{22}N_{a,Y} & F_{32}N_{a,Y} \\ F_{13}N_{a,Z} & F_{23}N_{a,Z} & F_{33}N_{a,Z} \\ F_{13}N_{a,Y} + F_{12}N_{a,Z} & F_{23}N_{a,Y} + F_{22}N_{a,Z} & F_{33}N_{a,Y} + F_{32}N_{a,Z} \\ F_{13}N_{a,X} + F_{11}N_{a,Z} & F_{23}N_{a,X} + F_{21}N_{a,Z} & F_{33}N_{a,X} + F_{31}N_{a,Z} \\ F_{12}N_{a,X} + F_{11}N_{a,Y} & F_{22}N_{a,X} + F_{21}N_{a,Y} & F_{32}N_{a,X} + F_{31}N_{a,Y} \end{bmatrix}. \tag{31}$$

Usually, the finite element shape functions are given in terms of the isoparametric coordinates $\boldsymbol{\xi} = \{\xi_1, \xi_2, \xi_3\}$, which are defined locally in a reference element. This permits the numerical integration of the linearized weak-form integrals using Gauss quadrature. The derivatives with respect to the material coordinates are then found by

$$\frac{\partial N_a(\mathbf{X})}{\partial \mathbf{X}} = \left(\frac{\partial \mathbf{X}}{\partial \boldsymbol{\xi}}\right)^{-\mathrm{T}} \frac{\partial N_a(\boldsymbol{\xi})}{\partial \boldsymbol{\xi}}; \quad \frac{\partial \mathbf{X}}{\partial \boldsymbol{\xi}} = \sum_{a=1}^{8} \mathbf{X}_a \otimes \frac{\partial N_a(\boldsymbol{\xi})}{\partial \boldsymbol{\xi}}. \tag{32}$$

Accordingly, the differential volume in the linearized weak-form integrals is computed as

$$d\Omega = J_0^{\boldsymbol{\xi}} \, \mathrm{d}\xi_1 \mathrm{d}\xi_2 \mathrm{d}\xi_3 \tag{33}$$

where $J_0^{\boldsymbol{\xi}} = \det(\partial \mathbf{X}/\partial \boldsymbol{\xi})$. Similarly, the differential surface $(d\Gamma)$ is found by using the two-dimensional form of Eq. (33).

5 Numerical examples

The $\mathbf{F}^*$ decomposition method proposed in this paper for modeling materially uniform but inhomogeneous bodies is assessed via a pure tension problem. The problem definition and the finite element mesh used are depicted in Fig. 2, where the pressure on the top of the bar is $p = 100\,\text{MPa}$. The following modified strain energy function is used:

$$W_U(\mathbf{C}^*) = \frac{1}{2}\mu_0(\text{tr}\mathbf{C}^* - 3) - \mu_0 \ln J^* + \frac{\lambda_0}{2}(\ln J^*)^2, \tag{34}$$

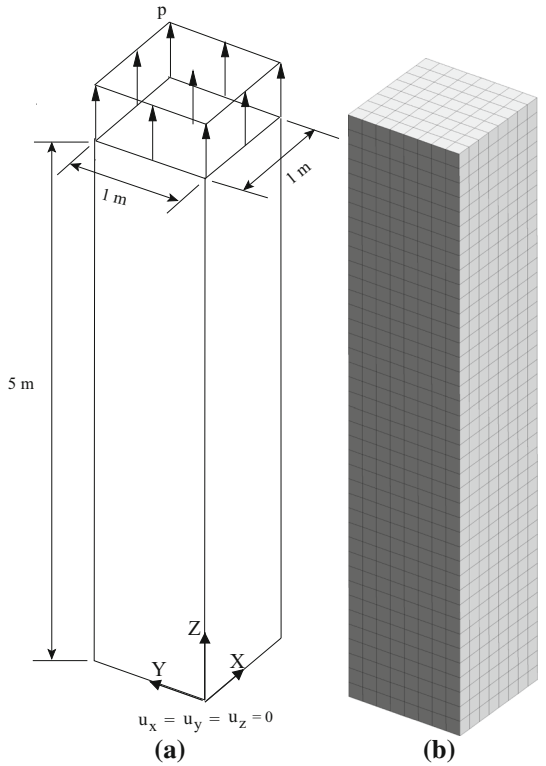

Fig. 2 Tension problem. **a** Geometry and boundary conditions, and **b** mesh of 8-node hexahedra

with material parameters $\mu_0 = 37.50937734\,\text{MPa}$ and $\lambda_0 = 74.79414764\,\text{MPa}$. The function $W_U(\mathbf{C}^*)$ defines the dislocated body in our framework when $\mathbf{K}$ is explicitly specified. The corresponding elastic material is obtained by setting $\mathbf{K} = \mathbf{I}$, which indicates the absence of defects, thereby leading to the expression

$$W(\mathbf{C}) = \frac{1}{2}\mu_0(\text{tr}\mathbf{C} - 3) - \mu_0 \ln J + \frac{\lambda_0}{2}(\ln J)^2. \tag{35}$$

In the numerical calculations, when the elastic body, material or solution is referred, we mean the outcome of the numerical solution based on Eq. (35) with the same values for the material parameters used in Eq. (34).

In the numerical examples, we use the Cauchy stress tensor, the principal stresses, the principal stretches and the von Mises stress to analyze the numerical results. The Cauchy stress tensor is computed as

$$\boldsymbol{\sigma} = (1/J)\mathbf{F}\mathbf{S}\mathbf{F}^{\text{T}} = (1/J)\mathbf{F}\mathbf{K}\mathbf{S}^*\mathbf{K}^{\text{T}}\mathbf{F}^{\text{T}}. \tag{36}$$

The components of the Cauchy stress tensor are used to compute the principal stresses and the von Mises stress. On the other hand, the principal stretches are obtained from

$$L_i = \sqrt{\lambda_i^*}, \tag{37}$$

where λ_i^* is an eigenvalue of the modified right Cauchy–Green deformation tensor $\mathbf{C}^*$.

5.1 Fully dislocated bar

For the uniform reference field, we select [46]

$$\mathbf{K} = \begin{bmatrix} 1 & 0 & 0 \\ 0 & 1 & 0 \\ 0 & 0.016Z^2 & 1 \end{bmatrix}^{-1}. \tag{38}$$

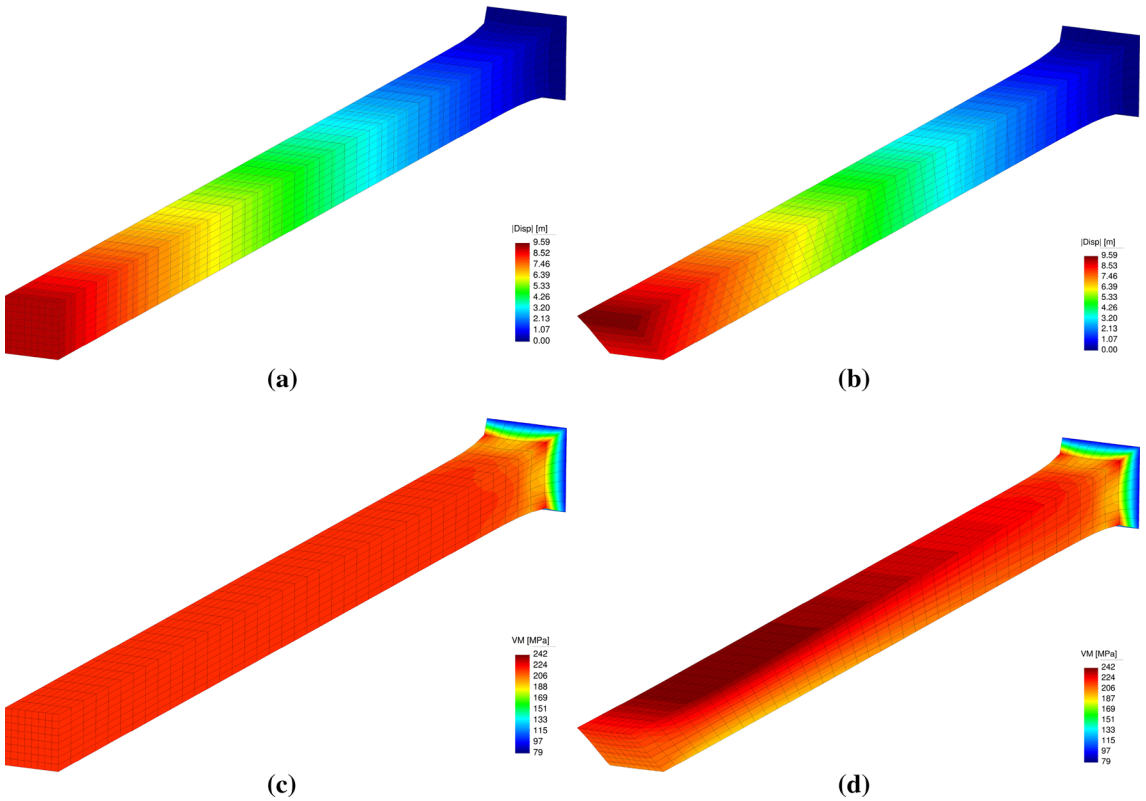

Fig. 3 Contour plots for the purely nonlinear elastic bar and the fully dislocated bar. **a** Magnitude of displacement for the purely nonlinear elastic bar, **b** magnitude of displacement for the fully dislocated bar, **c** von Mises stress for the purely nonlinear elastic bar, and **d** von Mises stress for the fully dislocated bar

This choice models a continuous distribution of edge dislocations with dislocated lines along the X direction and the Burgers vectors parallel to the Z direction, since the only nonvanishing component of the dislocation density tensor has the form

$$\alpha_{13} = 0.032Z. \tag{39}$$

So, we speak about dislocations distributed linearly in the medium. For inserting the field of defects in the code, the value of the uniform reference is specified at every Gauss point.

The contour plots of the displacement field are given in Fig. 3a, b. Figure 3a corresponds to the elastic problem, whereas Fig. 3b to the corresponding dislocated one. The presence of defects is reflected mainly on the top surface of the bar, where the dislocated body is much more displaced. This is expected since at higher points of the bar the inhomogeneity is larger due to the specific expression of $\mathbf{K}^{-1}$. The contour plots of the von Mises stress are given in Fig. 3c, d. Figure 3c corresponds to the purely elastic problem, whereas Fig. 3d to the dislocated counterpart. Stresses are concentrated near the boundary surface of the bar lying on plane ZX, whereas on the opposite side of the bar the stresses appear to have lower values.

For highlighting the way the axial displacement and the principal stress are distributed along the bar, the line $\overline{AC}$ shown in Fig. 4 is chosen. Figure 5a shows the way the axial displacement drifts from the elastic solution as higher points are reached along the line $\overline{AC}$, where the inhomogeneity increases. The dashed line corresponds to the purely elastic problem, whereas the continuous curve to the dislocated one. Figure 5b shows the way the axial displacement changes with the load steps at point B. The dislocated body results in axial displacement that grows faster with the load steps for this point. So, it is apparent that the difference between the displacement solutions of the dislocated and the elastic problems becomes more intense as the upper part of the bar is reached, where the inhomogeneity is larger.

For the way the principal stress varies with the distance along the line $\overline{AC}$, we refer to Fig. 6a. Up to the height of approximately 0.35 m in the bar, there are small differences between the elastic and the dislocated solution. But at higher locations, the differences become significant. Figure 6b shows the way the principal

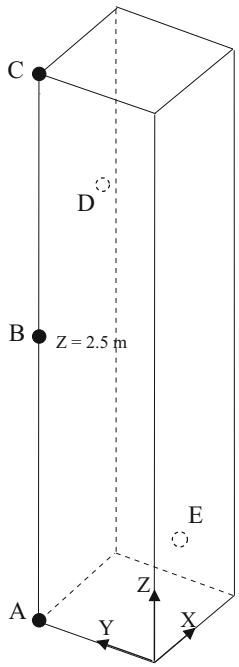

Fig. 4 Locations of the measure points for the fully dislocated bar. Edge defined by point *A* and *C* is used to measure stress and displacement along the length of the bar; points *B*, *D* and *E* are used to measure the evolution of the stress with the number of load steps and to measure the stress versus stretch response curve; and point *C* is used to measure the evolution of the displacement with the number of load steps

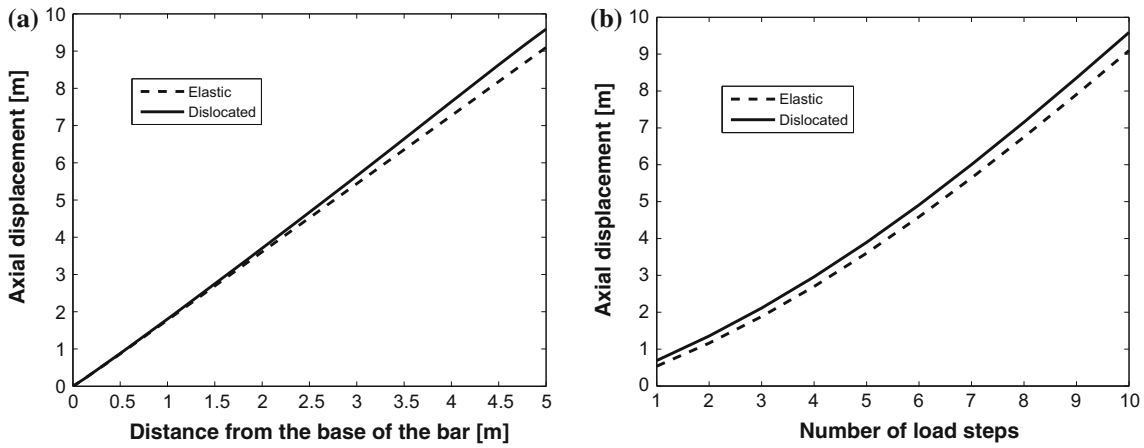

Fig. 5 Displacement response curves for the purely nonlinear elastic bar and the fully dislocated bar. **a** Axial displacement along the length of the bar (edge $\overline{AC}$), and **b** evolution of the axial displacement with the number of load steps at point B

stress is altered with the load steps for the point B of the bar. The dislocated body results in larger stresses than its elastic counterpart, and this difference increases with the load steps.

The principal stress versus principal stretch response diagram at point B is given in Fig. 7. The curve is constructed as a function of the load steps, namely the first point on the left of each curve corresponds to the pair (stress, stretch) that results from the mechanical response at the first load increment, whereas the last point on the right of each curve corresponds to the pair (stress, stretch) that results at the last load increment. It is observed that the presence of the defects does not alter the form of the nonlinearity, but in the dislocated body, the location of the pair (stress, stretch) on the curve is ahead from the corresponding pair of the purely elastic body. So, if a definite yield limit exists, it signifies that the initiation of plasticity is approached faster by the dislocated model.

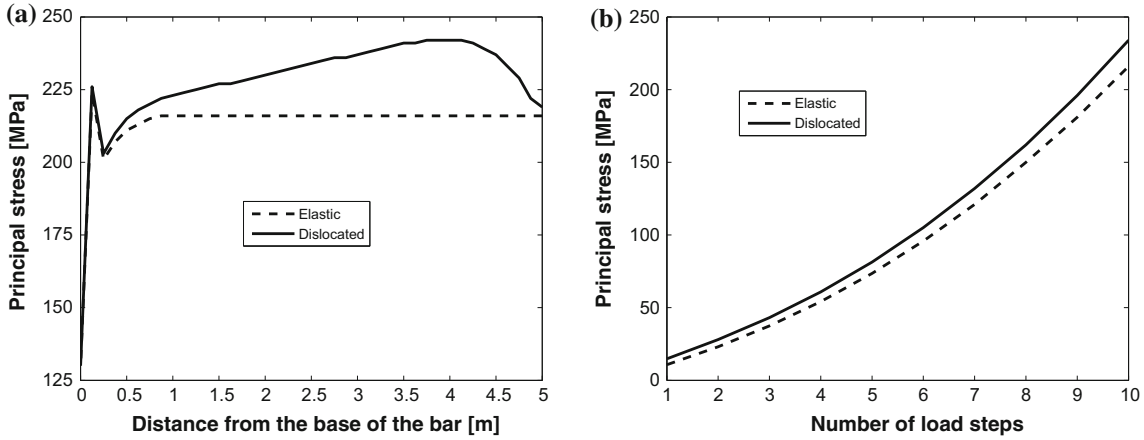

Fig. 6 Principal stress response curves for the purely nonlinear elastic bar and the fully dislocated bar. **a** Principal stress along the length of the bar (edge $\overline{\mathrm{AC}}$), and **b** evolution of the principal stress with the number of load steps at point B

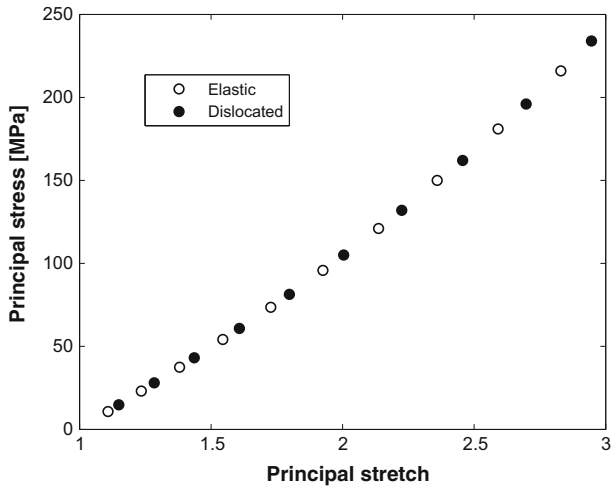

Fig. 7 Principal stress versus principal stretch response curves at point B for the purely nonlinear elastic bar and the fully dislocated bar. The first point on the left of each curve corresponds to the first load increment, whereas the last point on the right of each curve to the last load increment

Of course, due to the inhomogeneity of the model, every point of the bar should be examined separately. We present a pictorial akin to the one in Fig. 7 for the arbitrarily chosen points D and E of the dislocated bar. The principal stress versus principal stretch response curve for these points is depicted in Fig. 8, where the elastic solution is not presented. It is noted that the location of the pair (stress, stretch) on the curve of point B is ahead from the corresponding pair on the curves of points D and E. So, if a definite homogeneous yield limit for the whole body exists, this would be approached faster at point B of the bar highlighting the localization zones that occur due to the presence of the internal stresses on the as-received body. The latter can be explained for this particular case by observing the nonuniformity of the stretch field in Fig. 9, where the location of point E is surrounded by smaller stretches than for point D. On the other hand, point B is located near the region that exhibits the largest stretches, thereby explaining the order of the data for points B, D and E in Fig. 8.

So, a homogeneous yield condition of the form

$$\sigma_1 = W,$$

where σ_1 is the principal stress and W is a limiting value, fails to identify the regions where localization is to occur after yielding. It predicts yielding, but not where yielding occurs. Thus, the main outcome from the previous numerical results is that the presence of the defects induces changes in the way that principal stresses change with principal strains pointwise. So, if there is a definite homogeneous yield limit for the material, this is approached faster by the dislocated model. This is due to the presence of internal stresses as the result of

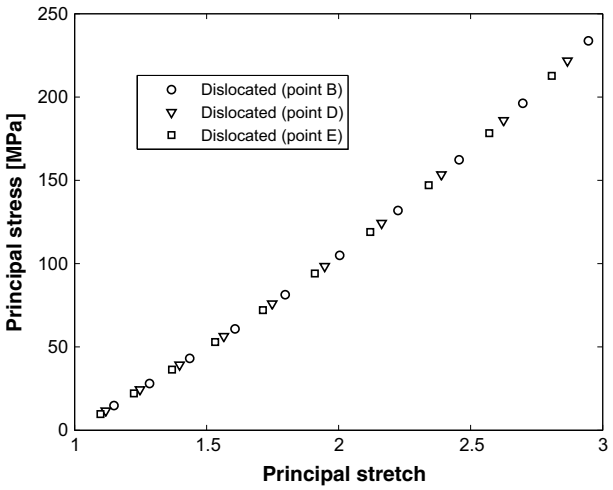

Fig. 8 Principal stress versus principal stretch response curves at points *B*, *D*, *E* for the purely nonlinear elastic bar and the fully dislocated bar. The first point on the left of each curve corresponds to the first load increment, whereas the last point on the right of each curve to the last load increment

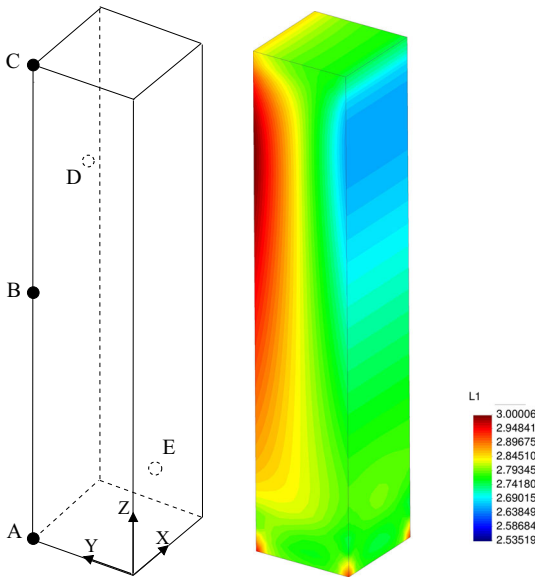

Fig. 9 Depiction of the nonuniformity of the principal stretch field in the fully dislocated bar. The location of point E is surrounded by smaller stretches than for point *D*. Point *B* is located near the region that exhibits the largest stretches

dislocations on the as-received body. Also, it appears that a homogeneous yield limit is approached faster by some points (and therefore regions) of the material, while other points remain in the elastic regime. This way plastic zones would only appear in those parts of the material that reached the yield limit. Even though our framework does not allow passage to the plastic regime (motion of dislocations), the present analysis exhibits how plastic zones and localization of deformation occur at the initiation of yielding. We underline that the localization of the kind meant above is due to internal stresses on the as-received body due to preexisting dislocations.

5.2 Bar with a single edge dislocation

For modeling only one dislocation, we specify the uniform reference field only to a set of Gauss points that discretely constitute a line threading the medium. So, by using the expression

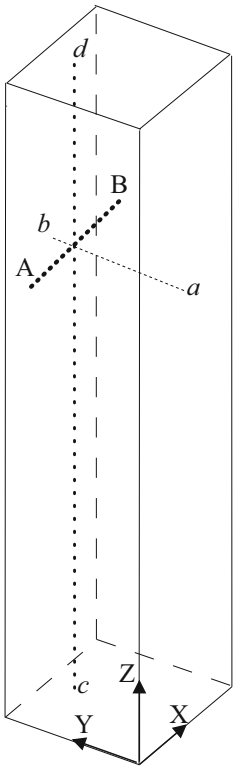

Fig. 10 Edge dislocation defined by $\overline{AB}$ for the single edge dislocated bar problem. Lines $\overline{ab}$ and $\overline{cd}$ are used to measure the principal stress

$$\mathbf{K} = \begin{bmatrix} 1 & 0 & 0 \\ 0 & 1 & 0 \\ 0 & 0.08Z^2 & 1 \end{bmatrix}^{-1}, \tag{40}$$

we model one edge dislocation in the X direction with the Burgers vector parallel to the Z direction. The dislocated line is the line $\overline{AB}$ shown in Fig. 10. The nontrivial component of the dislocation density tensor is

$$\alpha_{13} = 0.016Z. \tag{41}$$

Theoretically, the modeling of only one dislocation under Noll's framework would require the use of distributions in the components of the uniform reference. We bypass the use of distributions by specifying the uniform reference to every Gauss point that discretely constitutes the edge dislocation. This is strictly needed due to numerics since the weak-form integrals of the finite element method are computed numerically using Gauss quadrature. The location of the end points of the dislocated line is $A = (0, 0.8486, 3.7236)$ and $B = (1, 0.8486, 3.7236)$.

A convergence analysis is provided to validate the finite element mesh depicted in Fig. 2b, which is the mesh used in the present numerical examples. To this end, the dislocated line is kept fixed while the mesh is refined. Since an analytical solution is not available for the problem at hand, the results of one mesh are compared with those of the previous mesh. Thus, a refined mesh is deemed to be converged if its associated results do not differ much from those of the previous refinement. Figure 11 presents the convergence analysis for the principal stress measured along the dislocated line $\overline{\mathrm{AB}}$ and along the line $\overline{cd}$. A mesh of 3,321 nodes, which corresponds to the mesh depicted in Fig. 2b, proves to be sufficient in terms of convergence. The stress analyses follow.

Figure 12 shows the contour plots for the purely nonlinear elastic bar and its dislocated analog. The stress contours are provided at a cut through the plane that contains the dislocation. Of course, for the purely elastic problem, there is no dislocation, but the plane is the same for comparison purposes. By measuring the von Mises stress, we conclude that stresses are concentrated at the vicinity of the dislocated line, while at the same time there are regions where the stresses are smaller than those of the corresponding elastic problem.

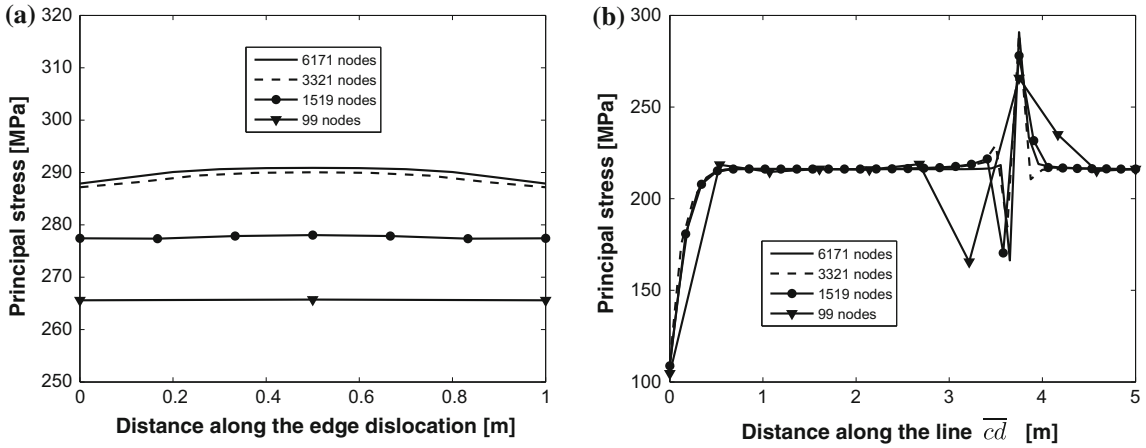

Fig. 11 Convergence study for the single edge dislocated bar. **a** Principal stress along the edge dislocation $\overline{\mathrm{AB}}$, and **b** principal stress along the line $\overline{cd}$

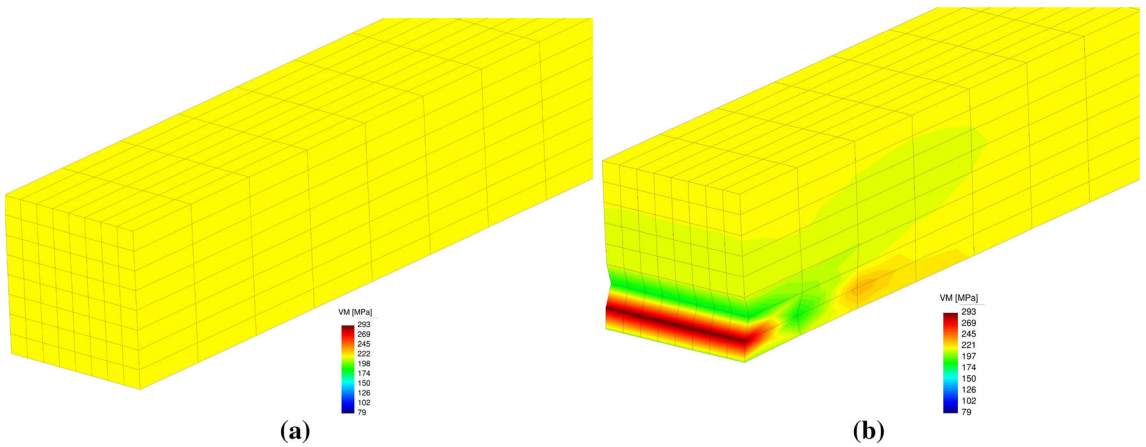

Fig. 12 Contour plots for the purely nonlinear elastic bar and the single edge dislocated bar. The figure shows a cut through the plane that contains the edge dislocation. **a** von Mises stress for the purely nonlinear elastic bar, and **b** von Mises stress for the single edge dislocated bar

The fact that along the dislocated line stresses are concentrated is also depicted in Fig. 13a. The continuous line corresponds to the dislocated solution, whereas the dashed one to the elastic solution. For the dislocated bar, stresses of approximately 290 MPa are obtained, whereas for the elastic bar somewhat less than 220 MPa.

The principal stress along the line $\overline{ab}$ is presented in Fig. 13b. The present method predicts finite values for the stresses nearby the dislocated line. The principal stress along the line $\overline{cd}$ is depicted in Fig. 14, where again bounded stresses are predicted near the dislocated line.

It is worth mentioning that the case of a single screw dislocation in a neo-Hookean body has been examined by Rosakis and Rosakis [38], Acharya [1], Yavari and Goriely [53]. The work of Rosakis and Rosakis [38] models the defect as a line where the displacement suffers a jump. In our framework, by contrast, the elastic displacement is smooth throughout the body. The field of defects is introduced by the inhomogeneous Curl-not-free expression for $\mathbf{K}^{-1}$. Acharya [1], using notions from exterior calculus, evaluates the field of internal stresses in a neo-Hookean material with a single screw dislocation. Yavari and Goriely [53], after constructing the relaxed manifold of a material with a single screw dislocation, calculate the field of internal stresses. It is emphasized that in our framework an initially dislocated body is subjected to a tensional loading, and the outcome is compared with the purely elastic solution. Thus, our approach differs from that of Acharya [1] and Yavari and Goriely [53] in the sense that the dislocated body is stressed externally.

Remark 1 We should mention that there are calculations for the stress field of an edge dislocation in an isotropic medium in the existing literature ([39], p. 143, Fig. 2). There, the authors calculate the stress field produced

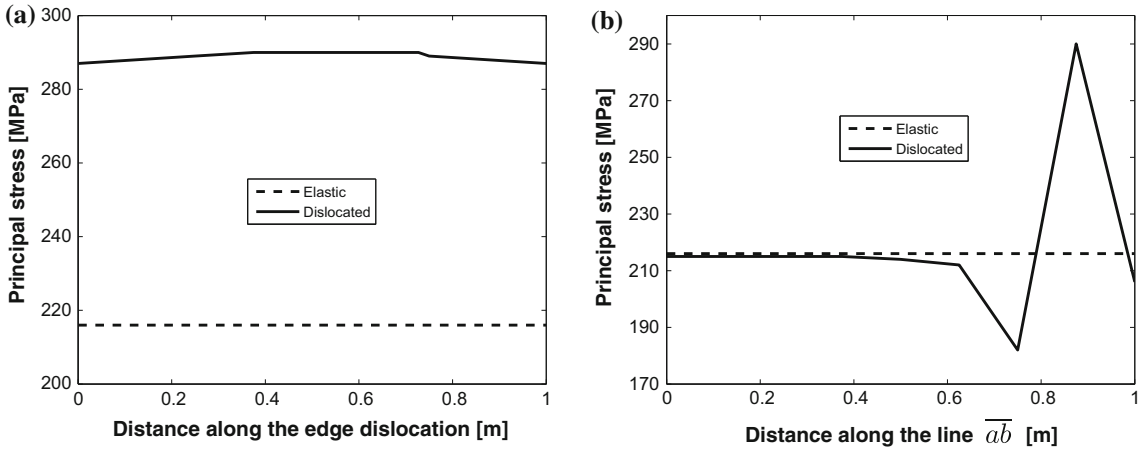

Fig. 13 Principal stress response curves for the purely nonlinear elastic bar and the single edge dislocated bar. **a** Principal stress along the edge dislocation $\overline{\mathrm{AB}}$, and **b** principal stress along the line $\overline{ab}$

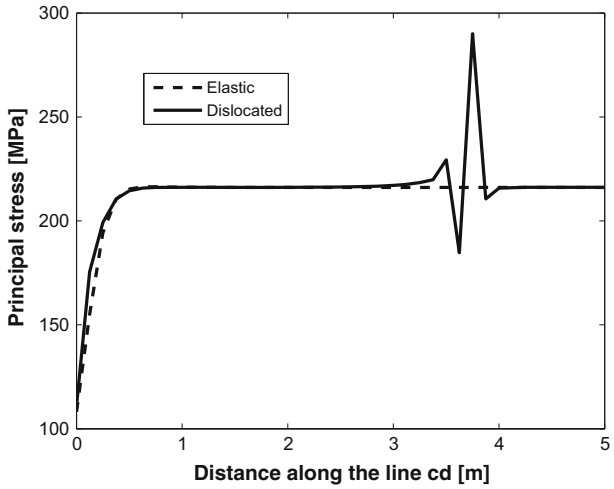

Fig. 14 Principal stress along the line $\overline{cd}$

by an edge dislocation in an isotropic medium without any external loading; essentially, these are the stresses necessary for the generation of the dislocation from an otherwise perfect body. In our approach, the field of the defects is assumed to exist, and we calculate how it interacts with the external loading. Even though a direct comparison is not possible, there is one qualitative result that is worth mentioning: The model in our approach predicts finite stresses as the dislocation line is approached. This is in line with Roy and Acharya [39], who also calculate a finite field of stresses near the dislocation, and in contrast to the theoretical results that predict an infinite stress field.

Remark 2 We remark that in the approach pursued in this paper, the dislocation is introduced as a line of inhomogeneity in the continuum. This makes the definition of the core region of the dislocation line unusual. There are no topological changes since the atoms are not displaced due to the presence of the defect; the defect is modeled as an inhomogeneity in the existing topology of the body.

5.3 Bar with a square dislocation loop

In this subsection, a closed square dislocation loop inside the bar is treated. The loop consists of edge segments (lines $\overline{bc}$ and $\overline{da}$ in Fig. 15) and screw segments (lines $\overline{ab}$ and $\overline{cd}$ in Fig. 15). The screw segment is used in order for the loop to be closed. For the edge dislocations (lines $\overline{bc}$ and $\overline{da}$) in the X direction with the Burgers

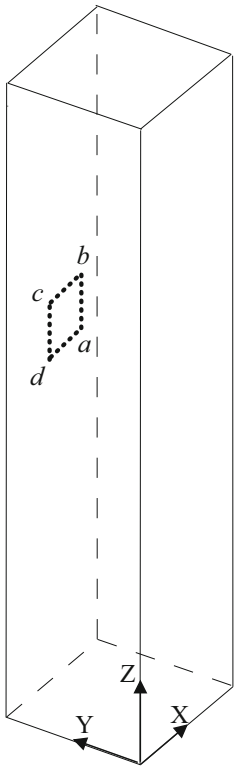

Fig. 15 Schematic picture of the square dislocation loop. The loop is defined by the segment $\overline{abcd}$

vectors parallel to the Z direction, the choice for the uniform reference is

$$\mathbf{K} = \begin{bmatrix} 1 & 0 & 0 \\ 0 & 1 & 0 \\ 0 & 0.08Z^2 & 1 \end{bmatrix}^{-1}. \tag{42}$$

On the other hand, for the screw segment (lines $\overline{ab}$ and $\overline{cd}$), the uniform reference is selected as [46]

$$\mathbf{K} = \begin{bmatrix} 1 & 0 & 0 \\ 0 & 1 & 0 \\ 0.08Y^2 & 1 & 1 \end{bmatrix}^{-1}. \tag{43}$$

This choice corresponds to a screw dislocation with both the Burgers vector and the edge dislocation along the Z direction since the only non-vanishing component of the dislocation density is

$$\alpha_{33} = 0.016Y. \tag{44}$$

In analogy with the approach of Subsection 5.2, the needed choices of the uniform reference are discretely specified at the Gauss points where the dislocation is assumed to be.

Figure 16 shows the contour plots for the principal stretch. Figure 16a shows the outcome for the purely elastic material and Fig. 16b for the body with the loop. It is observed that the stretch on the edge segments is larger than the stretch at the same location in the purely elastic bar, whereas near the screw segments, the differences between both models are not significant. Essentially, the upper part of the edge segment gives larger stretches. A similar observation can be made for the principal stress along the loop (Fig. 17).

A plot of the principal stress along the dislocation loop is pictured in Fig. 18. The dashed line corresponds to the elastic case, whereas the continuous line to the dislocated case. In general, it is seen that the presence of the defects is accompanied with larger principal stresses. The measurement of the distance along the loop starts at point a on the loop (see Fig. 15). In Fig. 18, the largest stresses occur on the edge segment $\overline{bc}$, followed by the stresses on $\overline{da}$ as it is readily seen in Fig. 17b.

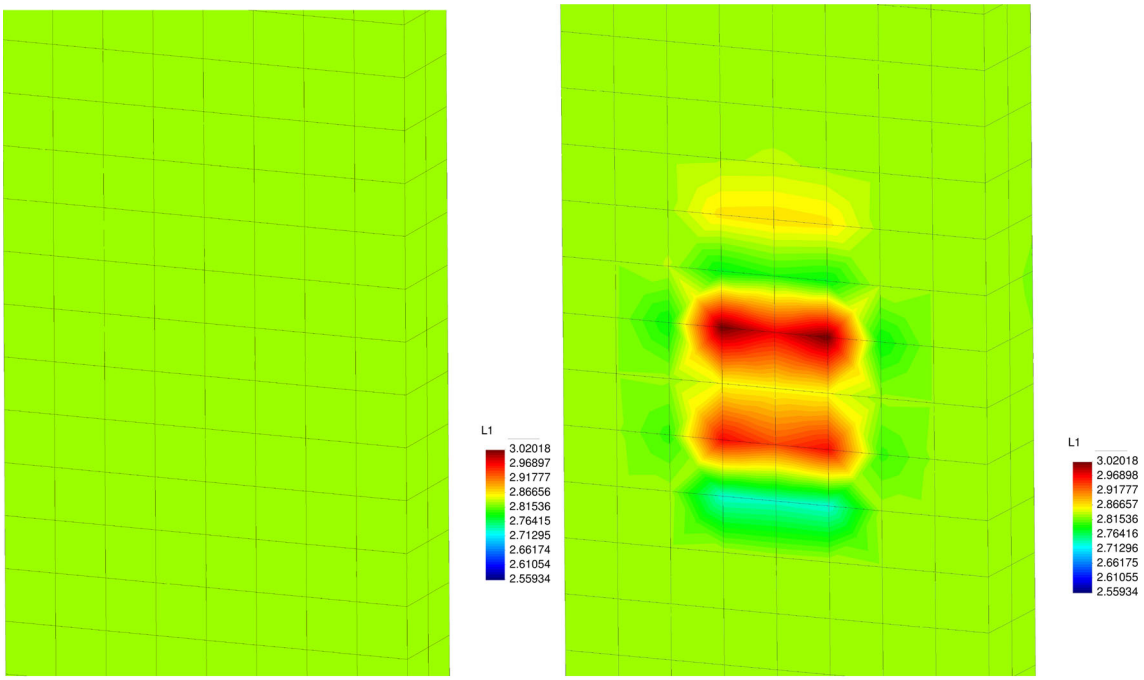

Fig. 16 Principal stretch contour plots for the bar with a square dislocation loop. **a** Principal stretch for the purely elastic problem, and **b** principal stretch for the bar with the loop

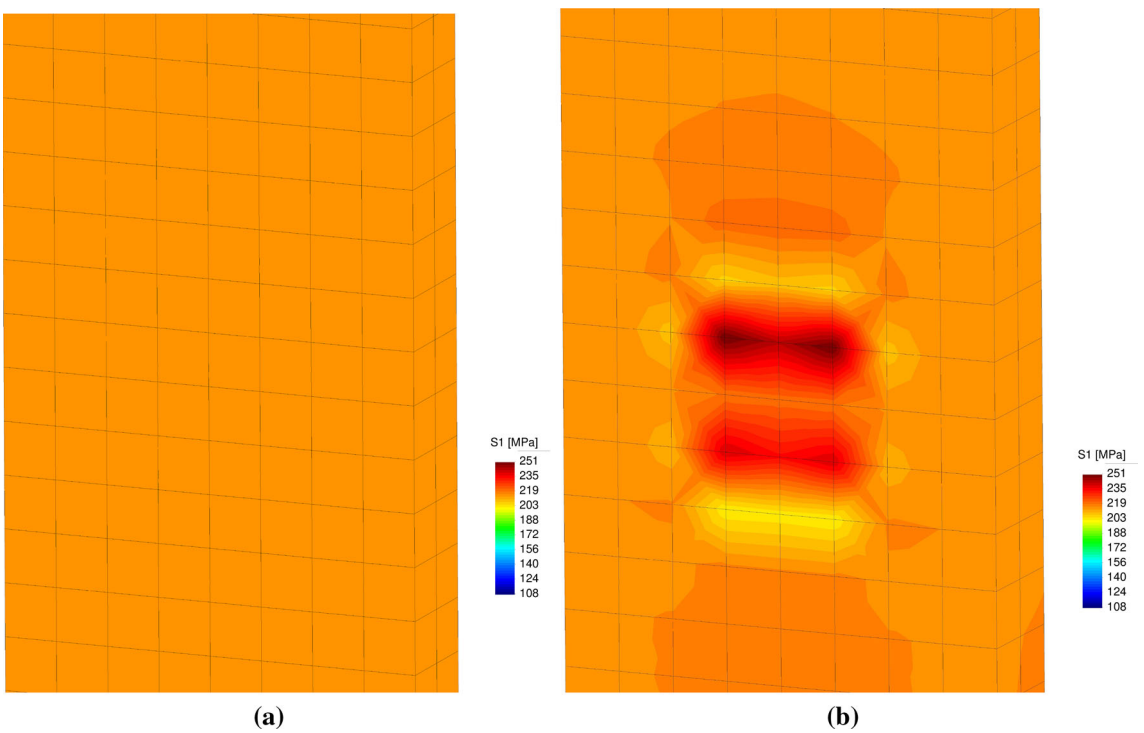

Fig. 17 Principal stress contour plots for the bar with a square dislocation loop. **a** Principal stress for the purely elastic problem, and **b** principal stress for the bar with the dislocation loop

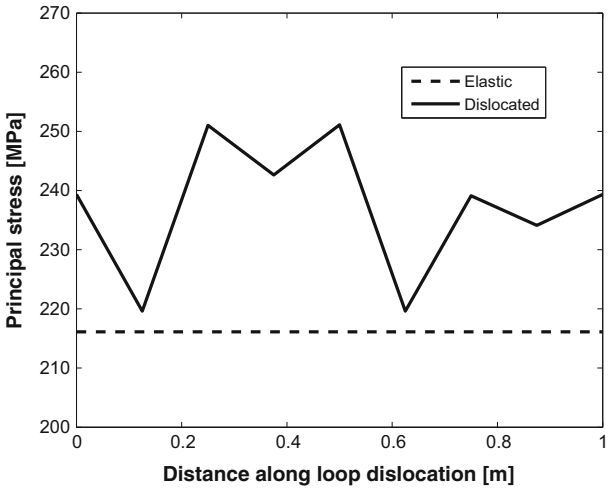

Fig. 18 Plot of the principal stress along the loop. The loop starts and ends at point *a*

6 Concluding remarks

The purpose of the present paper is to highlight the role played by a field of continuous distribution of dislocations in the elastic solution of a bar under tension. Essentially, we examine how a field of internal stresses that stems from dislocations affects the response of the body. For a continuous distribution of edge dislocations, it turns out that the principal stress grows faster in the dislocated body than in the elastic one. So, if a definite yield limit exists for both elastic and dislocated materials, it will be approached faster by the dislocated body. The source of this phenomenon is the presence of the internal stresses on the as-received body due to dislocations. Thus, for the problem at hand, the existence of a frozen field of dislocations results in larger stresses distributed in the body than in its elastic counterpart.

The distribution of these stresses is inherently inhomogeneous, which means there are zones where stresses are concentrated, while other zones are less affected by the presence of defects. So, by assuming the existence of a homogeneous yield limit for the body, there will be zones in the body where plasticity will start to develop, while other regions will remain in the elastic regime. For the discrete cases that were considered herein, the latter appears to be valid—the presence of the inhomogeneities leads to a concentration of stresses in the region near the defect. For the model at hand, the predicted stresses are finite.

The whole framework presented is valid for the case where the defects exist but are not allowed to move. The next step would be to consider the case where the dislocations on the as-received body are allowed to move with respect to the material, thereby producing plasticity. This issue would require the simultaneous solution of an equation that describes the evolution of the uniform reference, and it is a work in progress.

Acknowledgments The authors acknowledge valuable discussions with R. Bustamante (Santiago, Chile), V.K. Kalpakides (Ioannina, Greece) and G.I. Sfyris (Paris, France). A. Ortiz-Bernardin acknowledges the partial financial support of the Chilean National Fund for Scientific and Technological Development (Fondecyt) under Grant No. 11110389.

References

1. Acharya, A.: A model of crystal plasticity based on the theory of continuously distributed dislocations. J. Mech. Phys. Solids **49**, 761–784 (2001)
2. Acharya, A.: Driving forces and boundary conditions in continuum dislocation mechanics. Proc. R. Soc. A **459**, 1343–1363 (2003)
3. Acharya, A.: Constitutive analysis of finite field dislocation mechanics. J. Mech. Phys. Solids **52**, 301–316 (2004)
4. Acharya, A., Chapman, S.J.: Elementary observations on the averaging of dislocations mechanics: dislocation origin of aspects of anisotropic yield and plastic spin. In: Cazacu, O. (eds.) Linking Scales in Computations: From Microstructure to Macro-Scale Properties, IUTAM, Pensacola (2011)
5. Acharya, A., Roy, A.: Size effects and idealized dislocation microstructure at small scales: predictions of a phenomenological model of mesoscopic field dislocation mechanics: part I. J. Mech. Phys. Solid **54**, 1687–1710 (2006)
6. Belytschko, T., Gracie, R.: On XFEM applications to dislocations in problems with interfaces. Int. J. Plast. **23**, 1721–1738 (2007)

7. Bertram, A.: An alternative approach to finite plasticity based on material isomorphisms. Int. J. Plast. **15**, 353–374 (1999)
8. Bertram, A.: Finite thermoplasticity based on isomorphisms. Int. J. Plast. **19**, 2027–2050 (2003)
9. Bertram, A.: Elasticity and Plasticity of Large Deformations: An Introduction. 3rd edn. Springer, Berlin (2012)
10. Bilby, B.A., Bullough, R., Smith, E.: Continuous distribution of dislocations: a new application of the methods of non-Riemannian geometry. Proc. R. Soc. Lond. **231**, 263–273 (1955)
11. Bonet, J., Wood, R.: Nonlinear Continuum Mechanics for Finite Element Analysis. 2nd edn. Cambridge University Press, Cambridge (2008)
12. Cleja-Tigoiu, S., Soos, E.: Elastoviscoplastic models with relaxed configurations and internal variables. Appl. Mech. Rev. **43**, 131–151 (1990)
13. Dluzewski, P., Maciejewski, G., Jurczak, G., Kret, S., Laval, J.: Nonlinear FE analysis of residual stresses induced by dislocations in heterostructures. Comput. Mater. Sci. **29**, 379–395 (2004)
14. Dluzewski, P., Young, T.D., Dimitrakopulos, G.P., Kioseoglou, J., Komninou, P.: Nonlinear finite element and atomistic modelling of dislocations in heterostructures, ASM, vol 1. pp. 239–253. Springer, Berlin (2010)
15. Dluzewski, P., Young, T.D., Dimitrakopulos, G.P., Komninou, P.: Continuum and atomistic modelling of the straight mixed dislocation. Int. J. Multiscale Comput. Eng. **8**, 331–342 (2010)
16. Epstein, M.: Continuous distributions of dislocations in bodies with microstructure. J. Elast. **70**, 237–254 (2003)
17. Epstein, M.: The Geometrical Language of Continuum Mechanics. Cambridge University Press, Cambridge (2010)
18. Epstein, M., Elzanowski, M.: Material Inhomogeneities and Their Evolution. A Geometric Approach. Springer, Berlin (2007)
19. Epstein, M., de Leon, M.: Homogeneity conditions for generalized Cosserat media. J. Elast. **43**, 189–201 (1996)
20. Epstein, M., de Leon, M.: Geometrical theory of uniform Cosserat media. J. Geom. Phys. **26**, 127–170 (1998)
21. Epstein, M., Maugin, G.A.: The energy momentum tensor and material uniformity in finite elasticity. Acta Mech. **83**, 127–133 (1990)
22. Epstein, M., Maugin, G.A.: On the geometric material structure of anelasticity. Acta Mech. **115**, 119–136 (1996)
23. Gracie, R., Ventura, G., Belytschko, T.: A new fast method for dislocations based on interior discontinuities. Int. J. Numer. Methods Eng. **69**, 423–441 (2007)
24. Gracie, R., Oswald, J., Belytschko, T.: On a new extended finite element method for dislocations: core enrichment and nonlinear formulation. J. Mech. Phys. Solids **56**, 200–214 (2008)
25. Gupta, A., Steigmann, D.J., Stoelken, J.S.: On the evolution of plasticity and incompatibility. Math. Mech. Solids **12**, 583–610 (2007)
26. Gupta, A., Steigmann, D.J., Stoelken, J.S.: Aspects of the phenomenological theory of elastic–plastic deformation. J. Elast. **104**, 249–266 (2011)
27. Gurtin, M.: An Introduction to Continuum Mechanics. 1st edn. Academic Press, London (1981)
28. Kondo, K.: Non-Riemannian geometry of imperfect crystals from a macroscopic viewpoint. RAAG Mem. Unifying Study Basic Probl. Eng. Sci. Means Geom. **1**, 6–17 (1955)
29. Kosevich, A.M.: Crystal Dislocations and the Theory of Elasticity, vol 1.. pp. 33–142. North-Holland, Amsterdam (1979)
30. Kröner, E.: Continuum Theory of Defects. pp. 215–315. North-Holland, Amsterdam (1980)
31. Le, K.C., Stumpf, H.: Nonlinear continuum theory of dislocations. Int. J. Eng. Sci. **34**, 339–358 (1996)
32. Le, K.C., Stumpf, H.: On the determination of the crystal reference in the nonlinear continuum theory of dislocations. Proc. Math. Phys. Eng. Sci. **452**, 359–371 (1996)
33. Le, K.C., Stumpf, H.: Strain measures, integrability conditions and the theory of frame indifference in oriented media. Int. J. Solids Struct. **35**, 783–798 (1998)
34. Marsden, J.E., Hughes, T.J.R.: Mathematical Foundations of Elasticity. Dover, New York (1994)
35. Mura, T.: Continuous distribution of moving dislocations. Philos. Mag. **89**, 843–857 (1963)
36. Noll, W.: Materially uniform simple bodies with inhomogeneities. Arch. Ration. Mech. Anal. **27**, 1–32 (1967)
37. Palmov, V.: Large strain in viscoplasticity. Acta Mech. **125**, 129–139 (1997)
38. Rosakis, P., Rosakis, A.J.: The screw dislocation problem in incompressible finite elastostatics: a discussion of nonlinear effects. J. Elast. **20**, 30–40 (1988)
39. Roy, A., Acharya, A.: Finite element approximation of finite field dislocation mechanics. J. Mech. Phys. Solids **53**, 143–170 (2005)
40. Roy, A., Acharya, A.: Size effects and idealized dislocation microstructure at small scales: predictions of a phenomenological model of Mesoscopic Field Dislocation Mechanics: Part II. J. Mech. Phys. Solids **54**, 1711–1743 (2006)
41. Sfyris, D.: Propagation of a plane wave to a materially unifom but inhomogeneous body. Z. Angew. Math. Phys. **62**, 927–936 (2011)
42. Sfyris, D.: Autoparallel curves and Riemannian geodesics for materially uniform but inhomogeneous elastic bodies. Math. Mech. Solids **19**, 152–167 (2014)
43. Sfyris, D.: Comparing the condition of strong ellipticity and the solvability of an elastic problem and the corresponding dislocated problem. Math. Mech. Solids **17**, 254–265 (2012)
44. Sfyris, D.: Replacing ordinary derivatives by gauge derivatives in the continuum theory of dislocations to compensate the action of the symmetry group. Mech. Res. Commun. **51**, 56–60 (2013)
45. Sfyris, D.: The role of the symmetry group in the non-uniqueness of a uniform reference. Case study: An isotropic solid body. Math. Mech. Solids **18**, 738–744 (2013)
46. Sfyris, D., Charalambakis, N., Kalpakides, V.K.: Continuously dislocated elastic bodies with a neo-Hookean like expression for the energy subjected to antiplane shear. J. Elast. **93**, 245–262 (2008)
47. Steinmann, P.: Views on multiplicative elastoplasticity and the continuum theory of dislocations. Int. J. Eng. Sci. **34**, 1717–1735 (1996)
48. Svendsen, B.: A thermodynamic formulation of finite deformation elastoplasticity with hardening based on the notion of material isomorphism. Int. J. Plast. **14**, 473–488 (1998)

49. Svendsen, B.: On the modelling of anisotropic elastic and inelastic material behaviour at large deformation. Int. J. Solids Struct. **38**, 473–488 (2001)
50. Wang, C.: On the geometric structure of simple bodies, a mathematical foundation for the theory of continuous distribution of dislocations. Arch. Ration. Mech. Anal. **27**, 33–94 (1967)
51. Willis, J.R.: Second order effects of dislocations in anisotropic crystals. Int. J. Eng. Sci. **5**, 171–190 (1967)
52. Y Basar, A.E.: Large inelastic strain analysis by multilayer shell element. Acta Mech. **141**, 225–252 (2000)
53. Yavari, A., Goriely, A.: Riemann–Cartan geometry of nonlinear dislocation mechanics. Arch. Ration. Mech. Anal. **205**, 59–118 (2012)